

Supporting Information for:

Restructuring of Mortise-and-Tenon Frameworks at Molecular Level

Yifei Li,[†] Fenglei Wang,[†] Shengchang Xiang,[†] Xi Fan,^{*,†} and Zhangjing Zhang^{*,†}

[†]Fujian Provincial Key Laboratory of Polymer Materials, College of Chemistry and Materials Science, Fujian Normal University, 32 Shangsang Road, Fuzhou 350007, P. R. China.

Email: fanxi@fjnu.edu.cn; z Zhang@fjnu.edu.cn.

Contents

Experimental Section	4
Material	4
Characterizations	4
Synthesis of MTF-4	4
Synthesis of MTF-5	4
General Methods for X-ray Crystallography.....	4
Fabrication of MTFs dispersed PDMS glasses	5
Z-scan measurements	5
Calculation of the nonlinear optical parameters	5
Table S1. Crystal data and structure refinement for MTF-4 and MTF-5	7
Table S2. Summary of experimental elastic moduli of Mortise-and-Tenon Frameworks materials.	8
Table S3. Summary of experimental elastic moduli of Cu-based crystal materials.....	8
Table S4. Summary of experimental elastic moduli of metal-organic frameworks (MOFs) materials, $M^n(n=1,2)$	8
Reference	9
Figure S1. The building unit of (a) MTF-4 and (b) MTF-5 . Atom color codes: Orange Cu; green F; red O; blue N; gray C; white H.....	11
Figure S2. Illustration of molecular chains of different layers in MTF-4 are staggered at a certain angle of 62°	11
Figure S3. Illustration of (a) the structure of adjacent chains and (b) the shortest Cu-Cu distance between adjacent layers molecular chains in MTF-4 . Atom color codes: Orange Cu; green F; red O; blue N; gray C; white H.	12
Figure S4. Illustration the ultimate stacking of mortise-and-tenon layers in MTF-4	12
Figure S5. Illustration of (a) the molecular chains pairing up to form thickened units through π - π interactions and (b) such thickened units further stacking in an offset pattern to construct a layer in MTF-5	13
Figure S6. (a) The structure of thickened chains and (b) the shortest Cu-Cu distance between adjacent molecular chains in MTF-5 . Atom color codes: Orange Cu; green F; red O; blue N; gray C; white H.	13
Figure S7. The Electrostatic Potential Surfaces (ESP) of the simplified models of (a) MTF-4 and (b) MTF-5	13
Figure S8. Structural illustration of the molecular chains of the adjacent layer assembling in a similar fashion but in an oblique straight orientation, locking the horizontally stacked molecular chains through mortise-and-tenon joints in MTF-5	14
Figure S9. Illustration the ultimate stacking of mortise-and-tenon frameworks in MTF-5	14
Figure S10. The $F\cdots H$ hydrogen bonds in (a) MTF-4 and (b) MTF-5	15
Figure S11. The XPS spectra of (a) MTF-4 and (b) MTF-5 , confirming valence state of the Cu atoms in both MTF-4 and (b) MTF-5 is +1.	15
Figure S12. The 001 crystallographic planes in the single crystals of (a) MTF-4 and (b) MTF-5 , which were identified by a Supernova single crystal diffractometer equipped with graphite-monochromatic Cu K radiation ($\lambda = 1.54178 \text{ \AA}$). The structure of (c) MTF-4 and (d) MTF-5 from the view of 001 crystallographic plane.	15
Figure S13. The PXRD patterns of (a) MTF-4 and (b) MTF-5 under different conditions, showing its	

stability in the air for at least 6 months.	16
Figure S14. The PXRD patterns of (a) MTF-4 and (b) MTF-5 at different temperatures.	16
Figure S15. shows the powder X-ray diffraction (PXRD) patterns of (a) MTF-4 and (b) MTF-5 after soaking in aqueous solutions of different pH values for 12 hours.	16
Figure S16. Powder X-ray diffraction of MTF-4 in different organic solutions.	17
Figure S17. Powder X-ray diffraction of MTF-5 in different organic solutions.	17
Figure S18. The UV-vis spectra of MTF-4 and MTF-5	17
Figure S19. The photograph of PDMS , MTF-4/PDMS (0.1%) and MTF-5/PDMS (0.1%).	18
Figure S20. Illustration of the stability of MTF-4 in PDMS verified by SCXRD of recovered single crystal wrapped in PDMS glass.	18
Figure S21. Illustration of the stability of MTF-5 in PDMS verified by SCXRD of recovered single crystal wrapped in PDMS glass.	19
Figure S22. The PXRD patterns of (a) MTF-4 and (b) MTF-5 after treatment with laser.	19
Figure S23. The IR spectrum (a) MTF-4 and (b) MTF-5 after treatment with laser.	20
Figure S24. The repeatability of third-order NLO responses for (a) MTF-4 and (b) MTF-5	20

Experimental Section

Material

All the reagents and solvents employed are purchased commercially and used as received without further treatment. Copper(I) oxide, 4,4'-Bipyridine, 4-Fluorobenzoic Acid, 3,4-Difluorobenzoic acid, Diphenylsilane, were purchased from Adamas-beta, while acetonitrile was bought from Sinopharm Chemical Reagent Beijing. All the reagents and solvents employed are purchased commercially and used as received without further treatment.

Characterizations

We collected the Fourier transform infrared spectroscopy (FTIR) data on a PerkinElmer Spectrum 100 FT-IR Spectrometer at ATR mood. Powder X-ray diffraction (PXRD) data analysis were collected on a Rigaku Mini Flex II diffractometer using CuK α radiation ($\lambda = 1.54056 \text{ \AA}$) in the 2θ range of $5\text{--}30^\circ$ with a scanning rate of 5°min^{-1} . AFM measurements were obtained using a Dimension Icon microscope (Bruker, US) in tapping mode in air, with a scan rate of 0.5 Hz. Surface topographies and phase images of the crystals glued to the cover glass were scanned in tapping mode. X-ray photoelectron spectroscopy (XPS) were recorded using a Escalab 250Xi instrument from Thermo Scientific equipped with an Al K α microfocused X-ray source and the C1s peak at 284.8 eV as internal standard.

Synthesis of MTF-4: Copper(I) oxide (0.12 g, 0.84 mmol), 3,4-Difluorobenzoic acid (0.6 g, 3.79 mmol), and 4,4'-Bipyridine (0.04 g, 0.256 mmol) were weighed in a 20 mL colorless clear glass bottle, 9 mL of acetonitrile was added, and then 60uL Diphenyl silane was added. The mixed solution was sealed and heated at 85°C for 1 day. The red-black plate crystals were obtained. The product was washed by Ethanol. (Yield: 17% based on Copper(I) oxide). Elemental analysis for $(\text{C}_{24}\text{H}_{14}\text{Cu}_2\text{F}_4\text{N}_2\text{O}_4)_n$, Calcd (%): C, 48.25; H, 2.36; O, 10.72. Found: C, 48.61; H, 2.51; O, 10.56.

Synthesis of MTF-5: Copper(I) oxide (0.12 g, 0.84 mmol), 4-Fluorobenzoic Acid (0.4 g, 2.85 mmol), and 4,4'-Bipyridine (0.056 g, 0.359 mmol) were weighed in a 20 mL colorless clear glass bottle, 8 mL of acetonitrile was added, and then 100uL Diphenylsilane was added. The mixed solution was sealed and heated at 85°C for 1 day. The black block-shape crystals were obtained. The product was washed by Ethanol. (Yield: 38% based on Copper(I) oxide). Elemental analysis for $(\text{C}_{24}\text{H}_{16}\text{Cu}_2\text{F}_2\text{N}_2\text{O}_4)_n$, Calcd (%): C, 51.34; H, 2.87; O, 11.40. Found: C, 51.74; H, 2.87; O, 11.53.

General Methods for X-ray Crystallography. The structure determination of **MTF-4** and **MTF-5** were collected on a Supernova single crystal diffractometer equipped with graphite-

monochromatic Cu K radiation ($\lambda = 1.54178 \text{ \AA}$) at 283K and 200K. Absorption correction was applied using SADABS.^[1] Using Olex2^[2], the structure was solved with the SHELXT^[3] structure solution program using Intrinsic Phasing and refined with the SHELXL^[3] refinement package using Least Squares minimisation. Crystal data and details of data collection and refinement of **MTF-4** and **MTF-5** were summarized in Table S1. CCDC 2406016 (**MTF-4**) and CCDC 2406017 (**MTF-5**) contain the supplementary crystallographic data for this paper. This data is provided free of charge by The Cambridge Crystallographic Data Centre.

Fabrication of MTFs dispersed PDMS glasses. PDMS glass were fabricated using Sylgard 184 (Dow Corning) by thoroughly mixing 10 parts bases to 1 part curing agent. The MTFs crystals were ground into MTFs powder (0.1%) and were mixed with the PDMS solution to form MTFs dispersed PDMS suspension. And then, the mixture suspension was added into a template and then put the template into a vacuum oven at 60°C for 3 hours. Last, the transparent and flexible MTFs/PDMS glasses were obtained.

Z-scan measurements. The nonlinear optical properties of the sample were evaluated using the Z-scan technique. The excitation light source was an Nd: YAG laser with a repetition rate of 10 Hz. The laser pulses (period, 5 ns; wavelength, 532 nm) were split into two beams with a mirror. The pulse energies at the front and back of the samples were monitored using energy detectors 1 and 2. All of the measurements were conducted at room temperature. The sample was mounted on a computer-controlled translation stage that shielded each sample along the z-axis.

Calculation of the nonlinear optical parameters. The relationship of the sample transmission and input laser intensity for a spatially Gaussian beam can be plotted from the open-aperture Z-scan curve. From the input laser pulse energy E_{in} and beam radius $\omega(z)$, the light fluence $F_{in}(z)$ at any position can be obtained. $F_{in}(z)$ is defined as

$$F_{in}(z) = \frac{4E_{in}\sqrt{\ln 2}}{\pi^2 \omega(z)^2}$$

Where $\omega(z)$ is defined as:

$$\omega(z) = \frac{\omega_0}{\left[1 + \left(\frac{z}{z_0}\right)^2\right]^{\frac{1}{2}}}$$

where ω_0 and z_0 are the light beam radius and the Rayleigh range, respectively, and z_0 is defined as:

$$z_0 = \frac{k\omega_0^2}{2}$$

Where k is defined as:

$$k = \frac{2\pi}{\lambda}$$

Table S1. Crystal data and structure refinement for **MTF-4** and **MTF-5**.

Compounds	MTF-4	MTF-5
CCDC	2406016	2406017
Empirical formula	(C ₂₄ H ₁₄ Cu ₂ F ₄ N ₂ O ₄) _n	(C ₂₄ H ₁₆ Cu ₂ F ₂ N ₂ O ₄) _n
Temperature/K	283.00(10)	199.8(3)
Crystal system	monoclinic	monoclinic
Space group	I2/a	P2 ₁ /n
a/Å	19.1711(5)	11.6320(3)
b/Å	14.3457(4)	7.8201(2)
c/Å	16.0551(4)	23.9312(4)
α/°	90	90
β/°	94.317(2)	92.220(2)
γ/°	90	90
Volume/Å ³	4403.0(2)	2175.23(9)
Z	8	4
ρ _{calc} /cm ³	1.796	1.714
μ/mm ⁻¹	3.027	2.881
F(000)	2368.0	1128.0
Radiation	Cu Kα (λ = 1.54184)	Cu Kα (λ = 1.54184)
Index ranges	-20 ≤ h ≤ 23, -6 ≤ k ≤ 17, -19 ≤ l ≤ 19	-14 ≤ h ≤ 13, -8 ≤ k ≤ 9, -29 ≤ l ≤ 26
Reflections collected	11997	12304
Independent reflections	4266 [R _{int} = 0.0872, R _{sigma} = 0.0599]	4220 [R _{int} = 0.0286, R _{sigma} = 0.0233]
Data/restraints/parameters	4266/0/343	4220/0/307
Goodness-of-fit on F ²	1.053	1.159
Final R indexes [I >= 2σ (I)]	R ₁ = 0.0686, wR ₂ = 0.1923	R ₁ = 0.0614, wR ₂ = 0.1626
Final R indexes [all data]	R ₁ = 0.0760, wR ₂ = 0.2032	R ₁ = 0.0644, wR ₂ = 0.1643
Largest diff. peak/hole/e Å ⁻³	0.87/-0.90	0.90/-1.00

Table S2. Summary of experimental elastic moduli of Mortise-and-Tenon Frameworks materials.

Name	Type	Young's modulus	Ref.
MTF-5	MTF	15.1 GPa	This work
MTF-4	MTF	6.1 GPa	This work
DOF-1	MTF	2.2 GPa	J. Am. Chem. Soc. 2024, 146, 12547–12555 ^[4]
DOF-2	MTF	0.9 GPa	J. Am. Chem. Soc. 2024, 146, 12547–12555 ^[4]

Table S3. Summary of experimental elastic moduli of Cu-based crystal materials.

Name	Type	Young's modulus	Ref.
HKUST-1	MOFs	6.45 GPa	ACS Appl. Mater. Interfaces, 2018, 10, 21079–21083 ^[5]
MFM-130	MOFs	7.79 Gpa	J. Am. Chem. Soc. 2016, 138, 3371–3381 ^[6]
MFM-131	MOFs	4.69 Gpa	J. Am. Chem. Soc. 2016, 138, 3371–3381 ^[6]
CuBDC NSs	MOFs	11.91 GPa	Adv. Sci. 2020, 7, 1903180 ^[7]
HKUST-1 monolith	MOF monoliths	9.3 GPa	Nat. Mater. 2017, 17, 174–179 ^[8]
COF-505	COFs	12.5 Gpa	Science, 2016, 351, 365-369 ^[9]
COF-524-Cu	COFs	3.41 Gpa	Chem, 2023, 9, 2509–2517 ^[10]
COF-525-Cu	COFs	2.38 Gpa	Chem, 2023, 9, 2509–2517 ^[10]

Table S4. Summary of experimental elastic moduli of metal-organic frameworks (MOFs) materials, $M^{n+}(n=1,2)$.

Name	Type	Young's modulus	Ref.
IMDFE	MOFs	2.2 GPa	J. Am. Chem. Soc. 2023, 145, 11258–11264 ^[11]
MOF-5	MOFs	2.7 Gpa	Phys. Rev. B, 2007 76, 184106 ^[12]
Cd-MOF	MOFs	11.3 GPa	Dalton Trans. 2016, 45, 6983–6989 ^[13]
ZIF-8	MOFs	3.7 Gpa	Nano Lett. 2019, 19, 6140–6143 ^[14]
^{CTN} MOF	MOFs	6.31 Gpa	Nature 2021, 598, 298–303 ^[15]
ZIF-71 monolith	MOF monoliths	1.67 Gpa	Mater. Today Nano, 2022, 17, 100166 ^[16]
ZIF-8 monolith	MOF monoliths	3.18 Gpa	Mater. Today Nano, 2022, 17, 100166 ^[16]
ag-MUV-24	MOF glasses	9.9 Gpa	J. Am. Chem. Soc. 2023, 145, 11258–11264 ^[11]
a _g -ZIF-4	MOF glasses	6.89 GPa	J. Am. Chem. Soc. 2019, 141, 1027–1034 ^[17]
a _g -ZIF-62	MOF glasses	6.58 Gpa	J. Am. Chem. Soc. 2019, 141, 1027–1034 ^[17]
a _g -ZIF-76	MOF glasses	6.29 Gpa	J. Am. Chem. Soc. 2019, 141, 1027–1034 ^[17]

Reference

- [1] Sheldrick, G. M. SADABS, Program for area detector adsorption correction. Institute for Inorganic Chemistry, University of Göttingen, Göttingen (Germany), 1996.
- [2] Dolomanov, O.V., Bourhis, L.J., Gildea, R.J, Howard, J.A.K. & Puschmann, H., OLEX2: a complete structure solution, refinement and analysis program. *J. Appl. Cryst.* 2009 **42**, 339-341.
- [3] Sheldrick, G.M. SHELXT – Integrated space-group and crystal-structure determination. *Acta Cryst. A* 2015, **71**, 3-8.
- [4] Sheng, X.; Wang, Z.; Sheng, G.; Zhu, C.; Xiao, D.; Shan, T.; Xiao, X.; Liu, M.; Li, G.; Zhu, Y.; Sessler, J. L.; Huang, F., Three-Dimensional Crystalline Organic Framework Stabilized by Molecular Mortise-and-Tenon Jointing. *J. Am. Chem. Soc.* 2024, **146**, 12547-12555.
- [5] Heinen, J.; Ready, A. D.; Bennett, T. D.; Dubbeldam, D.; Friddle, R. W.; Burch, N. C., Elucidating the Variable-Temperature Mechanical Properties of a Negative Thermal Expansion Metal–Organic Framework. *ACS Appl. Mater. Interfaces* 2018, **10**, 21079-21083.
- [6] Yan, Y.; Juriček, M.; Coudert, F.-X.; Vermeulen, N. A.; Grunder, S.; Dailly, A.; Lewis, W.; Blake, A. J.; Stoddart, J. F.; Schröder, M., Non-Interpenetrated Metal–Organic Frameworks Based on Copper(II) Paddlewheel and Oligoparaxylene-Isophthalate Linkers: Synthesis, Structure, and Gas Adsorption. *J. Am. Chem. Soc.* 2016, **138**, 3371-3381.
- [7] Huang, C.; Liu, C.; Chen, X.; Xue, Z.; Liu, K.; Qiao, X.; Li, X.; Lu, Z.; Zhang, L.; Lin, Z.; Wang, T., A Metal–Organic Framework Nanosheet - Assembled Frame Film with High Permeability and Stability. *Adv. Sci.* 2020, **7**, 1903180.
- [8] Tian, T.; Zeng, Z.; Vulpe, D.; Casco, M. E.; Divitini, G.; Midgley, P. A.; Silvestre-Albero, J.; Tan, J.-C.; Moghadam, P. Z.; Fairen-Jimenez, D., A sol–gel monolithic metal–organic framework with enhanced methane uptake. *Nat. Mater.* 2017, **17**, 174-179.
- [9] Liu, Y.; Ma, Y.; Zhao, Y.; Sun, X.; Gándara, F.; Furukawa, H.; Liu, Z.; Zhu, H.; Zhu, C.; Suenaga, K.; Oleynikov, P.; Alshammari, A. S.; Zhang, X.; Terasaki, O.; Yaghi, O. M., Weaving of organic threads into a crystalline covalent organic framework. *Science* 2016, **351**, 365-369.
- [10] Fritz, P. W.; Coskun, A., Weaving on a molecular scale: A challenge in two dimensions. *Chem*, 2023, **9**, 2509–2517.
- [11] León-Alcaide, L.; Christensen, R. S.; Keen, D. A.; Jordá, J. L.; Brotons-Alcázar, I.; Forment-Aliaga, A.; Mínguez Espallargas, G., Melttable, Glass-Forming, Iron Zeolitic Imidazolate Frameworks. *J. Am. Chem. Soc.* 2023, **145**, 11258-11264.
- [12] Bahr, D. F.; Reid, J. A.; Mook, W. M.; Bauer, C. A.; Stumpf, R.; Skulan, A. J.; Moody, N. R.; Simmons, B. A.; Shindel, M. M.; Allendorf, M. D., Mechanical properties of cubic zinc carboxylate IRMOF-1 metal-organic framework crystals. *Phys. Rev. B*, 2007, **76**, 184106.
- [13] Qu, X.-L.; Gui, D.; Zheng, X.-L.; Li, R.; Han, H.-L.; Li, X.; Li, P.-Z., A Cd(ii)-based metal–organic framework as a luminance sensor to nitrobenzene and Tb(iii) ion. *Dalton Trans.* 2016, **45**, 6983–6989.
- [14] Tiba, A. A.; Tivanski, A. V.; MacGillivray, L. R., Size-Dependent Mechanical Properties of a Metal–

- Organic Framework: Increase in Flexibility of ZIF-8 by Crystal Downsizing. *Nano Lett.* 2019, **19**, 6140-6143.
- [15] Meng, W.; Kondo, S.; Ito, T.; Komatsu, K.; Pirillo, J.; Hijikata, Y.; Ikuhara, Y.; Aida, T.; Sato, H., An elastic metal–organic crystal with a densely catenated backbone. *Nature* 2021, **598**, 298-303.
- [16] Tricarico, M.; Tan, J.-C., Mechanical properties and nanostructure of monolithic zeolitic imidazolate frameworks: a nanoindentation, nanospectroscopy, and finite element study. *Mater. Today Nano*, 2022, **17**, 100166.
- [17] Li, S.; Limbach, R.; Longley, L.; Shirzadi, A. A.; Walmsley, J. C.; Johnstone, D. N.; Midgley, P. A.; Wondraczek, L.; Bennett, T. D., Mechanical Properties and Processing Techniques of Bulk Metal–Organic Framework Glasses. *J. Am. Chem. Soc.* 2018, **141**, 1027-1034.

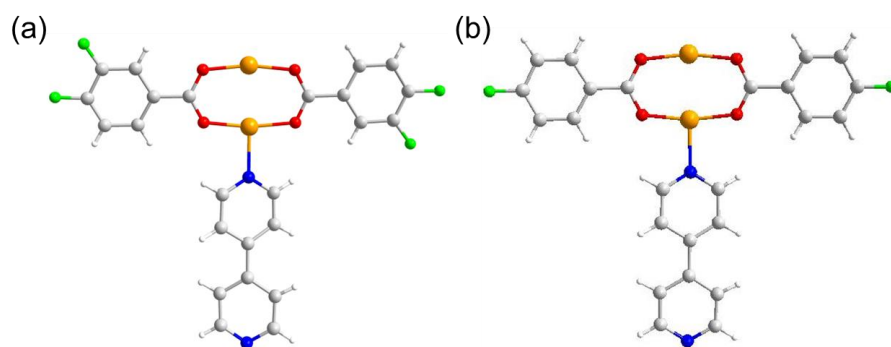


Figure S1. The building unit of (a) **MTF-4** and (b) **MTF-5**. Atom color codes: Orange Cu; green F; red O; blue N; gray C; white H.

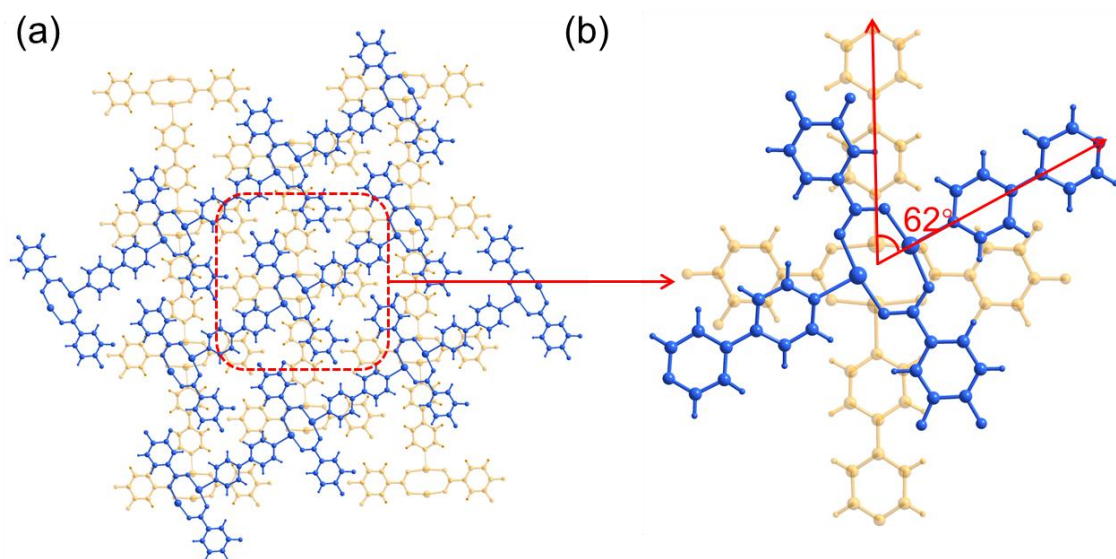


Figure S2. Illustration of molecular chains of different layers in **MTF-4** are staggered at a certain angle of 62° .

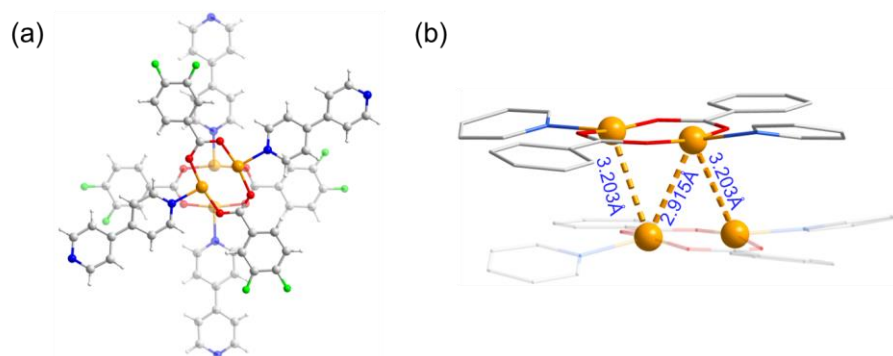


Figure S3. Illustration of (a) the structure of adjacent chains and (b) the shortest Cu-Cu distance between adjacent layers molecular chains in **MTF-4**. Atom color codes: Orange Cu; green F; red O; blue N; gray C; white H.

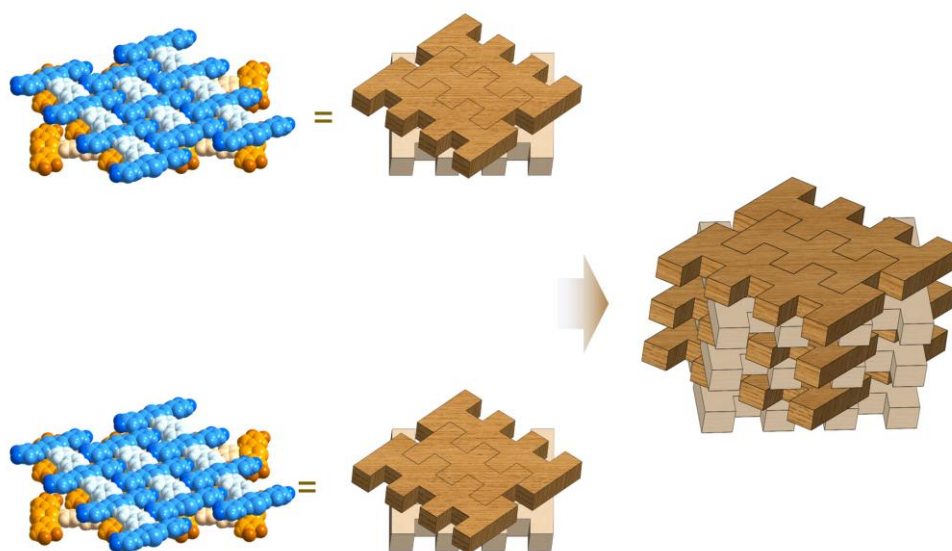


Figure S4. Illustration the ultimate stacking of mortise-and-tenon layers in **MTF-4**.

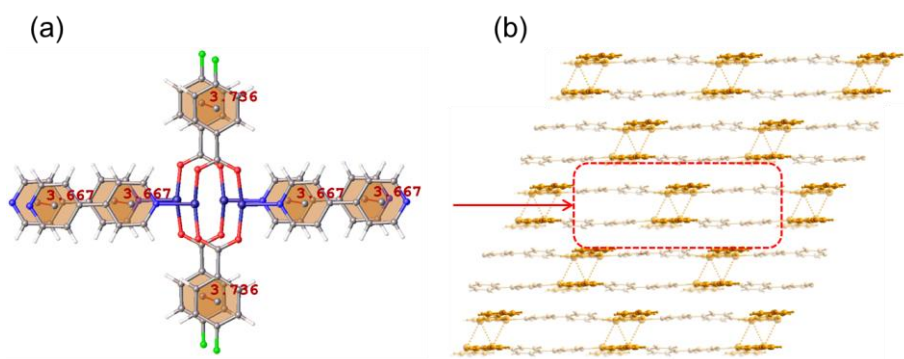


Figure S5. Illustration of (a) the molecular chains pairing up to form thickened units through π - π interactions and (b) such thickened units further stacking in an offset pattern to construct a layer in **MTF-5**.

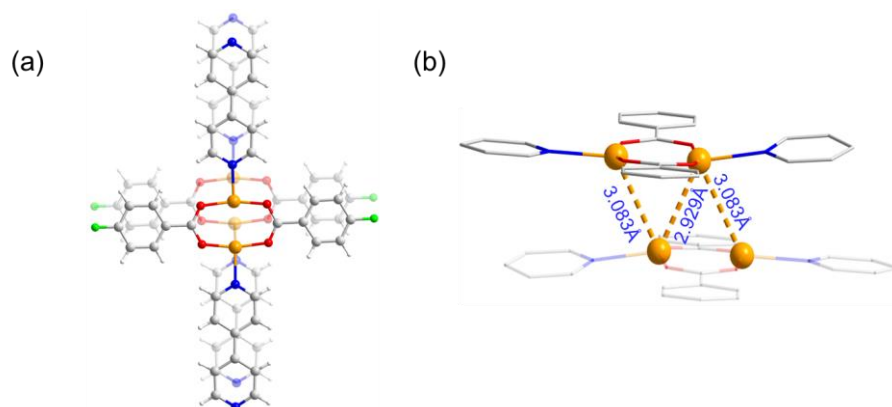


Figure S6. (a) The structure of thickened chains and (b) the shortest Cu-Cu distance between adjacent molecular chains in **MTF-5**. Atom color codes: Orange Cu; green F; red O; blue N; gray C; white H.

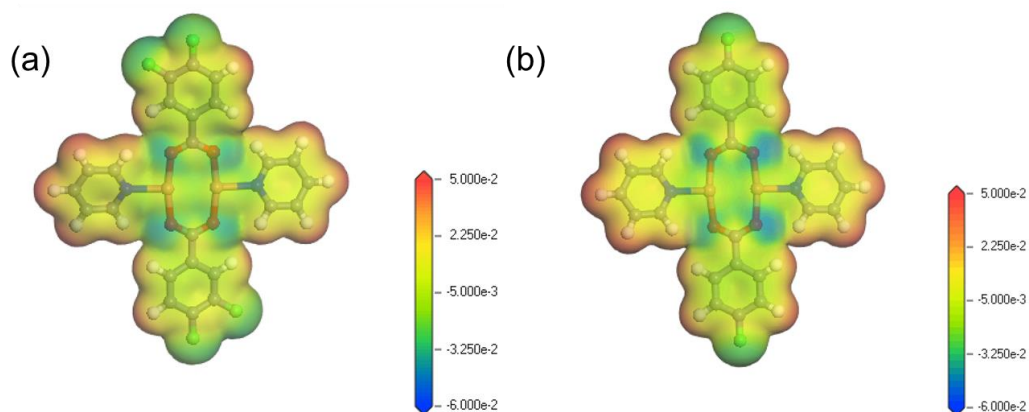


Figure S7. The Electrostatic Potential Surfaces (ESP) of the simplified models of (a) **MTF-4** and (b) **MTF-5**. The surface electrostatic potential of MTFs was computed using the DMol3 modules in Materials Studio. The calculations were performed using generalized gradient approximation (GGA) with the Becke-Lee-Yang-Parr (BLYP) exchange correlation functional. The convergence criteria of self-consistent field(SCF), energy tolerance, maximum force, and maximum displacement are 1.0×10^{-6} Ha/atom, 1.0×10^{-5} Ha/atom, 0.002 Ha/Å and 0.005 Å, respectively.

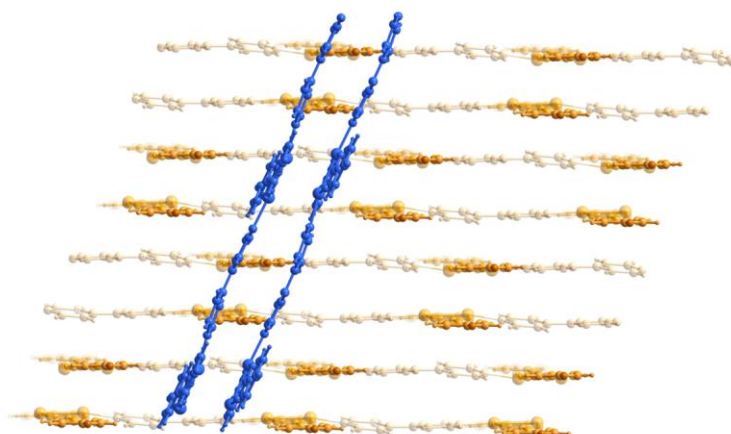


Figure S8. Structural illustration of the molecular chains of the adjacent layer assembling in a similar fashion but in an oblique straight orientation, locking the horizontally stacked molecular chains through mortise-and-tenon joints in **MTF-5**.

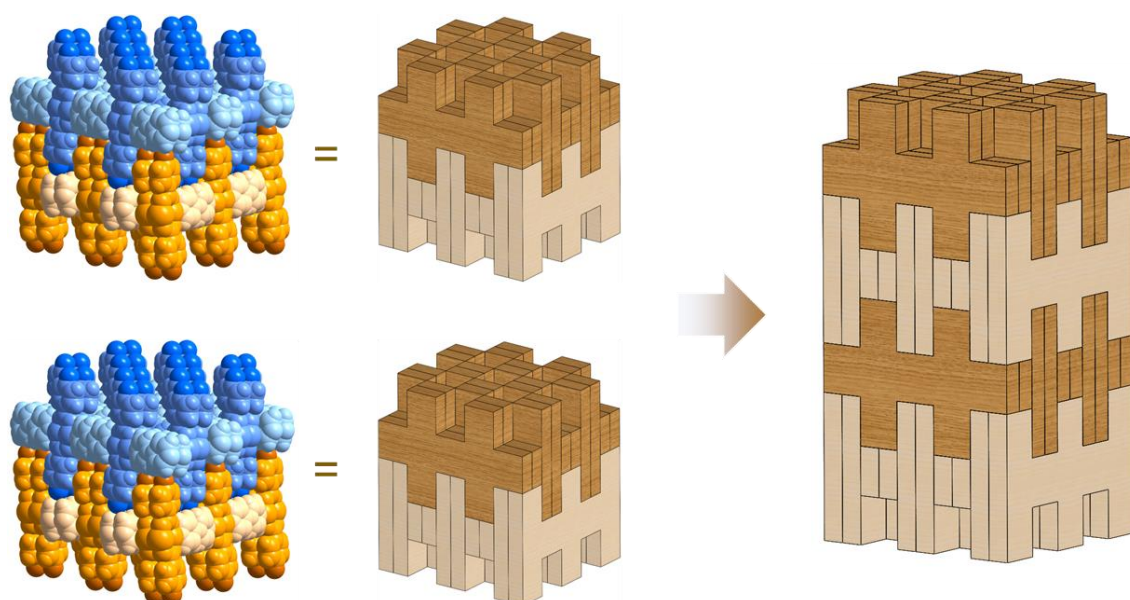


Figure S9. Illustration the ultimate stacking of mortise-and-tenon frameworks in **MTF-5**.

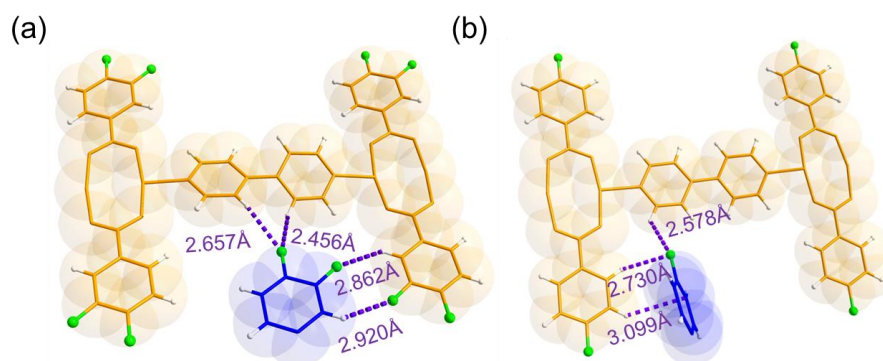


Figure S10. The F \cdots H hydrogen bonds in (a) **MTF-4** and (b) **MTF-5**.

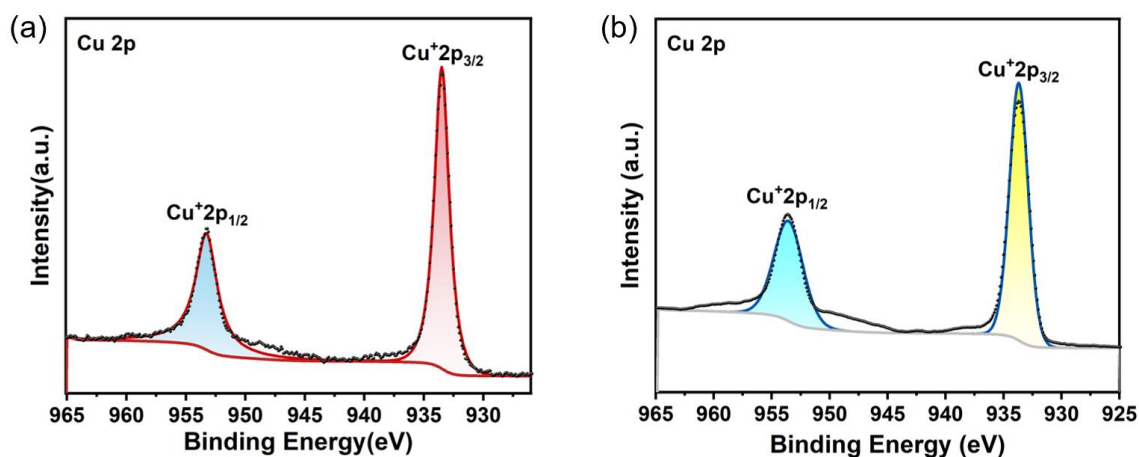


Figure S11. The XPS spectra of (a) **MTF-4** and (b) **MTF-5**, confirming valence state of the Cu atoms in both **MTF-4** and (b) **MTF-5** is +1.

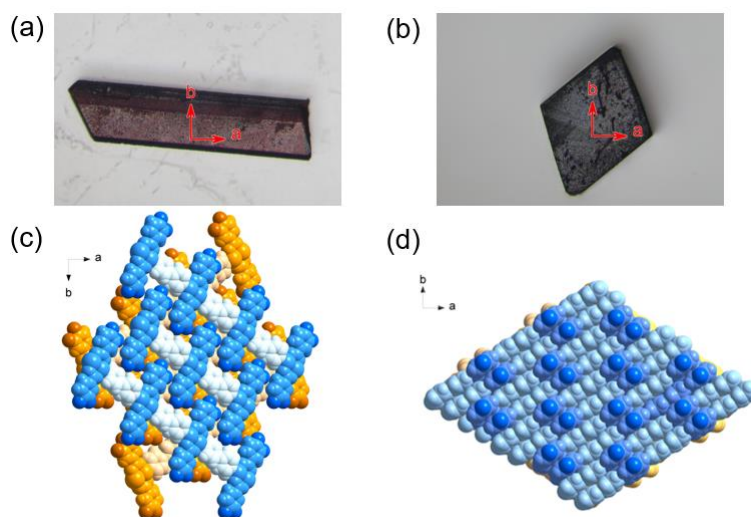


Figure S12. The 001 crystallographic planes in the single crystals of (a) **MTF-4** and (b) **MTF-5**, which were identified by a Supernova single crystal diffractometer equipped with graphite-monochromatic Cu K radiation ($\lambda = 1.54178 \text{ \AA}$). The structure of (c) **MTF-4** and (d) **MTF-5** from the view of 001 crystallographic plane.

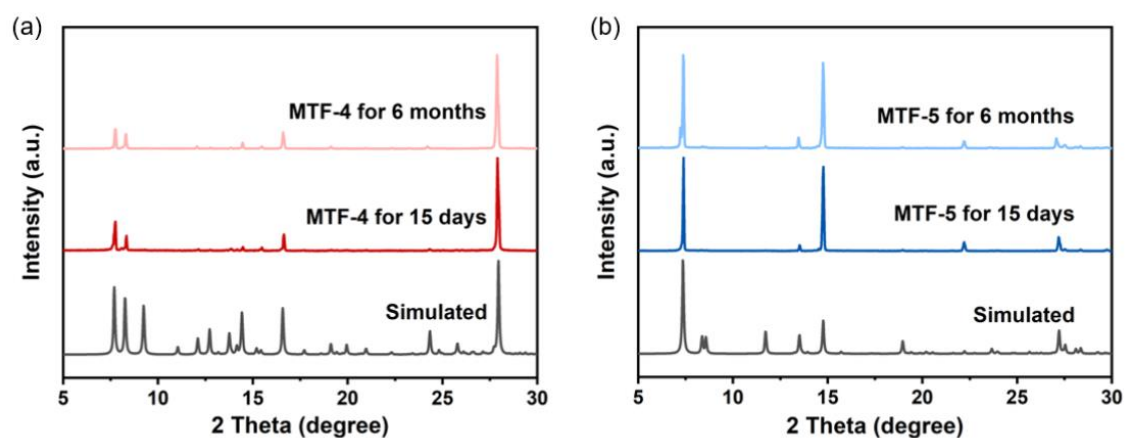


Figure S13. The PXR D patterns of (a) **MTF-4** and (b) **MTF-5** under different conditions, showing its stability in the air for at least 6 months.

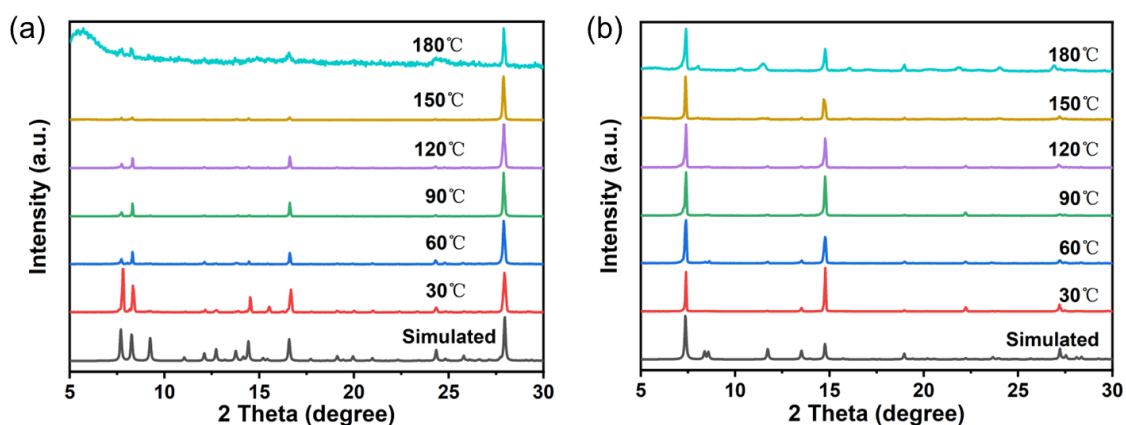


Figure S14. The PXR D patterns of (a) **MTF-4** and (b) **MTF-5** at different temperatures.

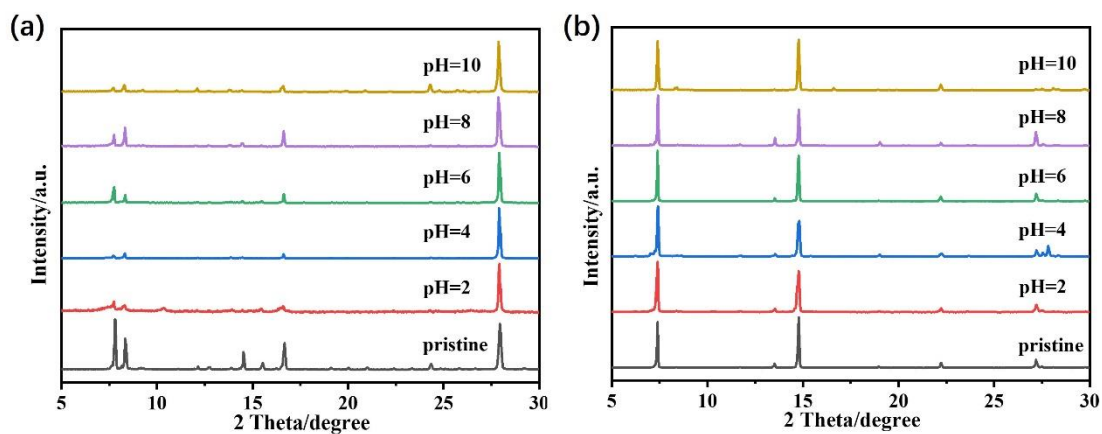


Figure S15. The powder X-ray diffraction (PXR D) patterns of (a) **MTF-4** and (b) **MTF-5** after soaking in aqueous solutions of different pH values for 12 hours.

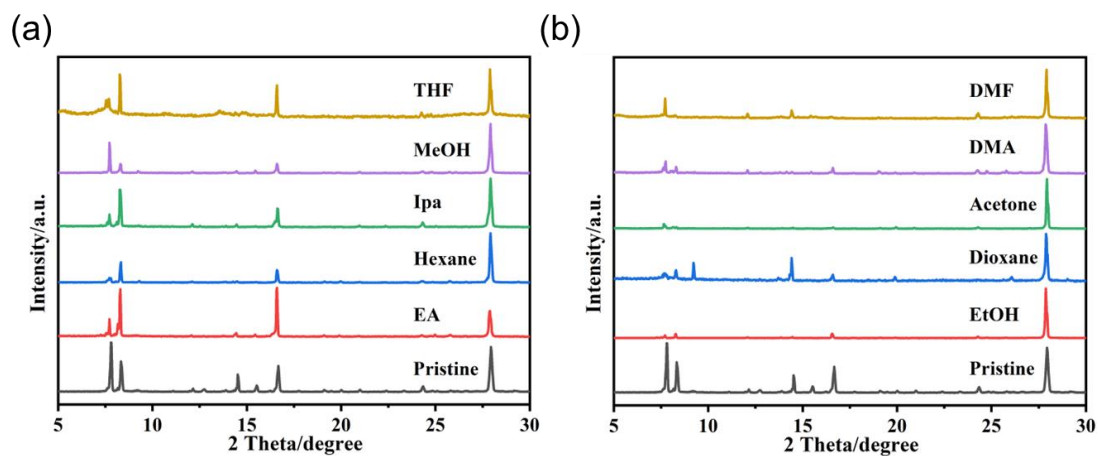


Figure S16. Powder X-ray diffraction of **MTF-4** in different organic solutions.

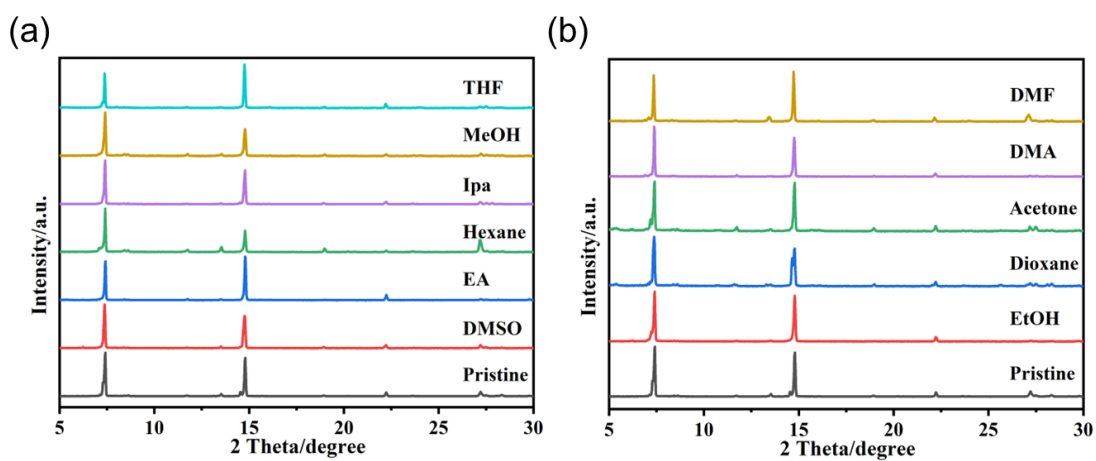


Figure S17. Powder X-ray diffraction of **MTF-5** in different organic solutions.

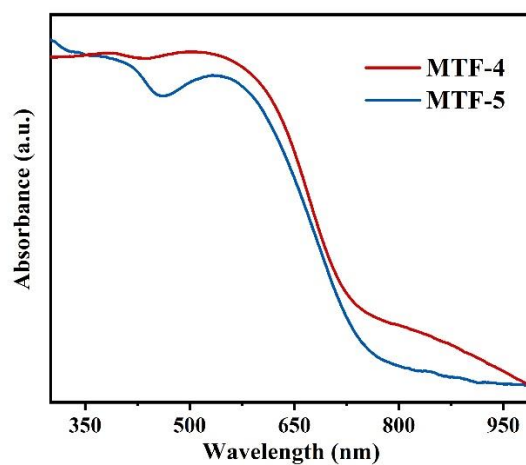


Figure S18. The UV-vis spectra of **MTF-4** and **MTF-5**.



Figure S19. The photograph of **PDMS**, **MTF-4/PDMS (0.1%)** and **MTF-5/PDMS (0.1%)**.

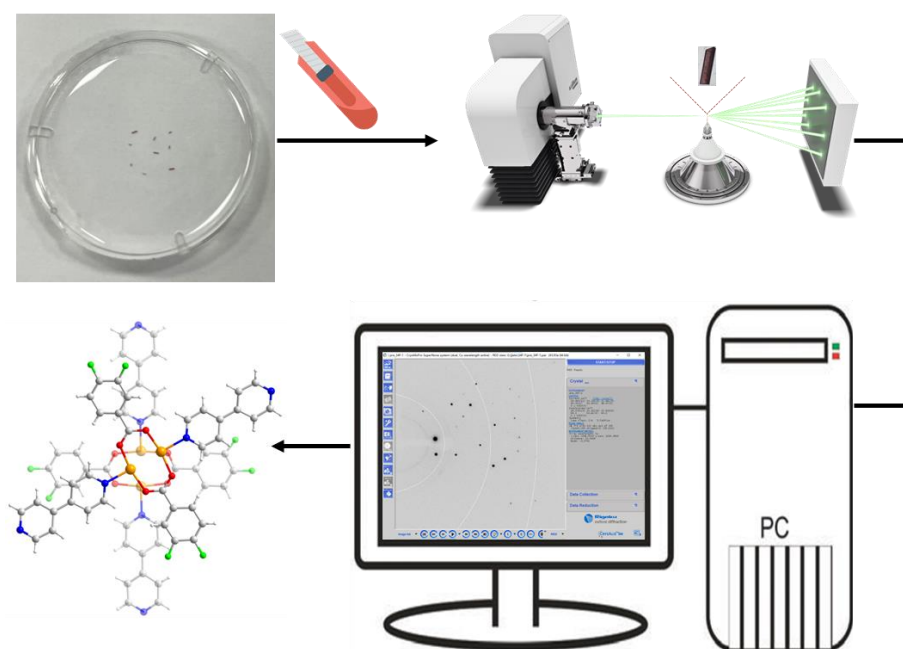


Figure S20. Illustration of the stability of **MTF-4** in PDMS verified by SCXRD of recovered single crystal wrapped in PDMS glass.

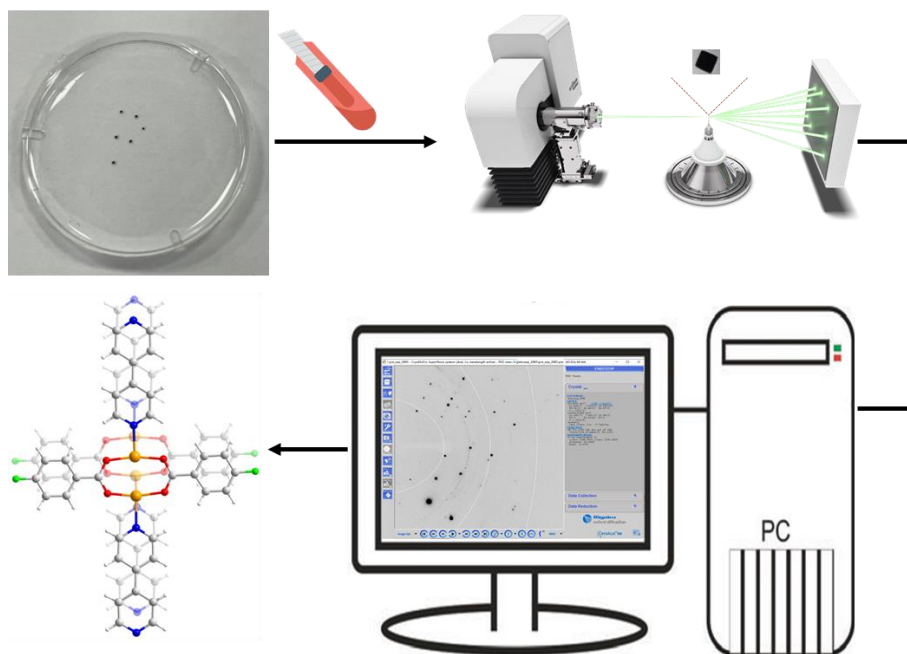


Figure S21. Illustration of the stability of **MTF-5** in PDMS verified by SCXRD of recovered single crystal wrapped in PDMS glass.

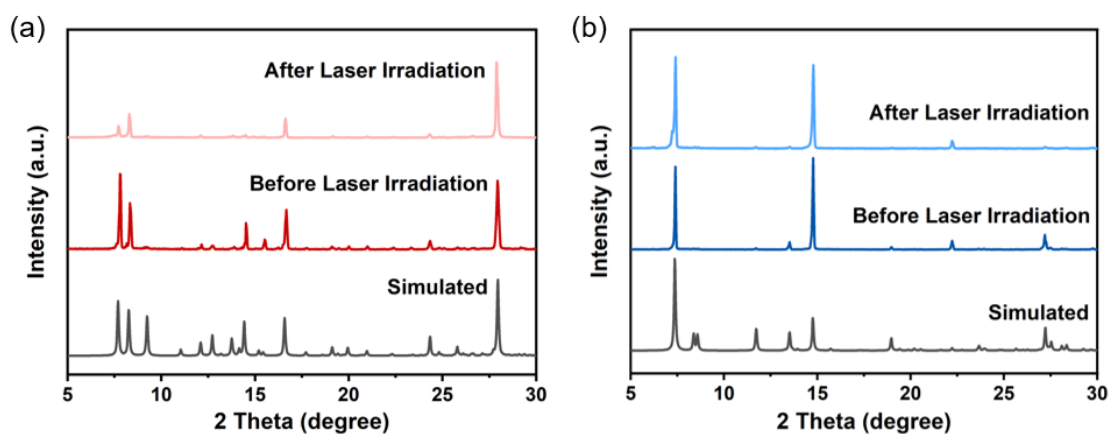


Figure S22. The PXRD patterns of (a) **MTF-4** and (b) **MTF-5** after treatment with laser.

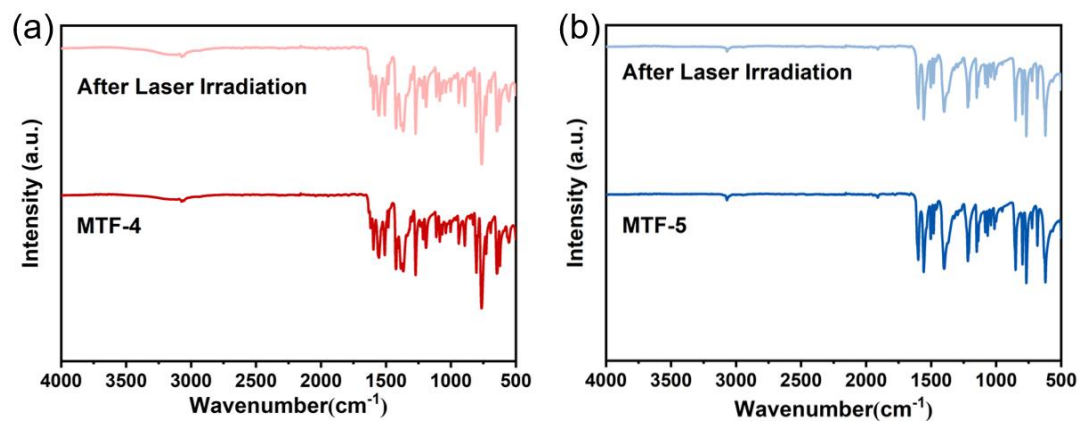


Figure S23 The IR spectrum (a) **MTF-4** and (b) **MTF-5** after treatment with laser.

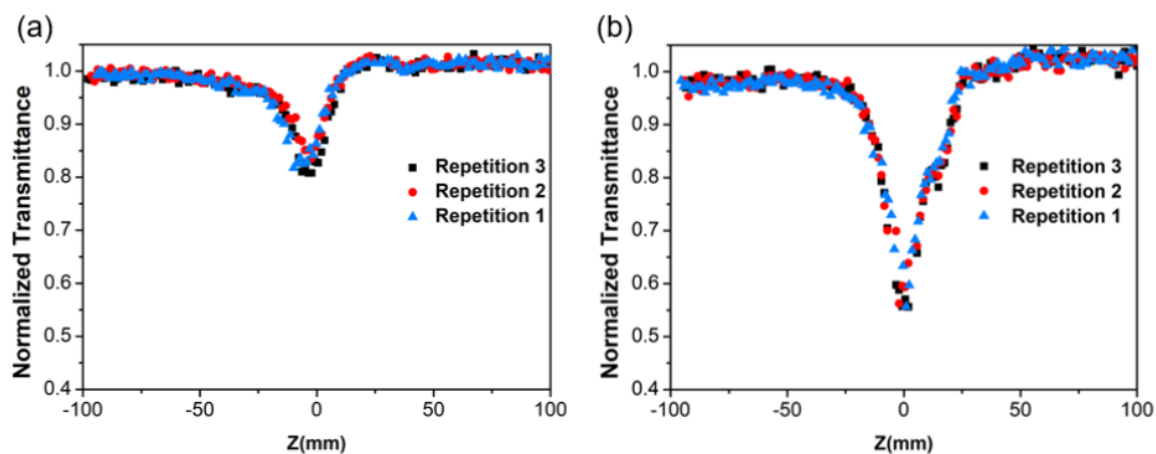


Figure S24. The repeatability of third-order NLO responses for (a) **MTF-4** and (b) **MTF-5**.